OPEN ACCESS

Deconvoluting Charge Transfer Mechanisms in Conducting Redox Polymer-Based Photobioelectrocatalytic Systems

To cite this article: N. Samali Weliwatte *et al* 2022 *J. Electrochem. Soc.* **169** 085501

Journal of The Electrochemical Society, 2022 **169** 085501

Deconvoluting Charge Transfer Mechanisms in Conducting Redox Polymer-Based Photobioelectrocatalytic Systems

N. Samali Weliwatte,[1] Olja Simoska,[1] Daniel Powell,[1] Miharu Koh,[1] Matteo Grattieri,[2,3,*] Luisa Whittaker-Brooks,[1] Carol Korzeniewski,[1,4] and Shelley D. Minteer[1,,z]**

[1]*Department of Chemistry, University of Utah, Salt Lake City, Utah 84112, United States of America*
[2]*Dipartimento di Chimica, Università degli Studi di Bari "Aldo Moro," Bari 70125, Italy*
[3]*IPCF-CNR Istituto per i Processi Chimico Fisici, Consiglio Nazionale delle Ricerche, Bari, 70125, Italy*
[4]*Department of Chemistry and Biochemistry, Texas Tech University, Lubbock, Texas 79409-1061, United States of America*

Poor electrochemical communication between biocatalysts and electrodes is a ubiquitous limitation to bioelectrocatalysis efficiency. An extensive library of polymers has been developed to modify biocatalyst-electrode interfaces to alleviate this limitation. As such, conducting redox polymers (CRPs) are a versatile tool with high structural and functional tunability. While charge transport in CRPs is well characterized, the understanding of charge transport mechanisms facilitated by CRPs within decisively complex photobioelectrocatalytic systems remains very limited. This study is a comprehensive analysis that dissects the complex kinetics of photobioelectrodes into fundamental blocks based on rational assumptions, providing a mechanistic overview of charge transfer during photobioelectrocatalysis. We quantitatively compare two biohybrids of metal-free unbranched CRP (polydihydroxy aniline) and photobiocatalyst (intact chloroplasts), formed utilizing two deposition strategies (*"mixed"* and *"layered"* depositions). The superior photobioelectrocatalytic performance of the *"layered"* biohybrid compared to the *"mixed"* counterpart is justified in terms of rate (D_{app}), thermodynamic and kinetic barriers ($H^{\neq}$, E_a), frequency of molecular collisions (D_0) during electron transport across depositions, and rate and resistance to heterogeneous electron transfer (k_0, R_{CT}). Our results indicate that the primary electron transfer mechanism across the biohybrids, constituting the unbranched CRP, is thermally activated intra- and inter-molecular electron hopping, as opposed to a non-thermally activated polaron transfer model typical for branched CRP- or conducting polymer (CP)-containing biohybrids in literature. This work underscores the significance of subtle interplay between CRP structure and deposition strategy in tuning the polymer-catalyst interfaces, and the branched/unbranched structural classification of CRPs in the bioelectrocatalysis context.

 [DOI: 10.1149/1945-7111/ac84b2]

Manuscript submitted May 24, 2022; revised manuscript received July 26, 2022. Published August 8, 2022.

Supplementary material for this article is available online

List of symbols

α	Transfer coefficient
$CD_{app}^{1/2}$	Concentration of redox-active species × apparent electron diffusion coefficient$^{1/2}$
CP	Conducting polymer
CRP	Conducting redox polymer
CV	Cyclic voltammetry
D	Diffusion coefficient
D_{app}	Apparent electron diffusion coefficient
DPSCA	Double potential step chronoamperometry
EIS	Electrochemical impedance spectroscopy
EPR	Electron paramagnetic resonance
ESEM	Environmental scanning electron microscopy
F	Faraday constant
h	Planck's constant
k_B	Boltzmann constant
k_0	Charge transfer rate constant
PANI	Polyaniline
PDHA	Polydihydroxyaniline
R	Gas constant
RP	Redox polymer
RDE	Rotating disk electrode
SEM	Scanning electron microscopy
T	Absolute temperature

Bioelectrocatalytic systems utilize highly selective, specific, reactive, and catalytically diverse biocatalysts that operate under mild conditions, to conduct electrochemical conversions on an electrode (e.g., biosolar and biofuel cells, biosensors, bioreactor, etc). Biocatalysts are typically encapsulated in multiple layers of lipid-based, electrically insulating membranes, which limit interfacial electron transfer, dissipating much of bioelectrocatalytically-harnessed energy in extraneous metabolic activity.[1–3] Direct electron transfer (DET) between biocatalysts and electrode surfaces is also limited by the spatial distribution of redox centers of the former (i.e., distance and relative orientations), based on the Marcus theory.[4,5] Therefore, the biotic-abiotic interface between the biocatalyst and electrode or modified-electrode surface is a critical factor determining bioelectrocatalytic efficiency in terms of (i) reducing contact resistance by increased physical affinity, (ii) facilitating electrochemical communication between biocatalysts and electrode, and (iii) providing physiological optima required by the metabolically dynamic biological entities.[1,6]

Increasingly sophisticated biocatalyst-electrode interfaces are designed, incorporating electrode surface modifications such as (i) "nano-structuring" to increase the load,[7] (ii) π–π stacking,[4,8] (iii) grafting functional groups on electrodes via covalent strategies and self-assembled monolayers,[5,9] (iv) bioscaffolding techniques to immobilize and orient biotic components, (v) hydrogel formation,[10,11] (vi) redox polymers and tethering, and (vii) conjugated polyelectrolytes, in order to electrochemically-*"wire"* physiologically incompatible biotic and abiotic components.[1,6] Among these, the use of redox polymers is an extremely attractive approach based on their structural, electronic tunability and versatility. Much scientific creativity can be exercised in the design of redox polymers for (i) efficient

*Electrochemical Society Member.
**Electrochemical Society Fellow.
[z]E-mail: minteer@chem.utah.edu

DET and mediated electron transfer (i.e., redox polymer as an electron shuttle) at the biocatalyst-electrode interface, (ii) biocatalyst immobilization and/or preservation of biocatalyst functionality, (iii) maintaining biocatalyst-electrode stability, and (iv) extending additional, case-specific functionalities to electrodes (e.g., multi-functional polymers in which solvation degree is governed by external triggers such as pH or temperature).[1,12]

Electrocatalytically significant polymers can be broadly categorized into: (i) *conducting polymers* (CPs), (ii) *redox polymers* (RPs),[13–15] and (iii) *conducting redox polymers* (CRPs), based on chemical structure and respective charge transfer mechanisms. CPs shuttle charge carriers through their π-conjugated backbones.[16] Disruptions in π-conjugation are compensated by strong electron-phonon interactions (i.e., polarons), which have lower mobility than free electrons due to higher effective mass.[17] Therefore, charge transfer in CPs occurs via a combination of polaron hopping through regions of disorder and bandlike transport through ordered regions.[18] Charge transfer in nonconjugated RPs is proposed to occur via a combination of the electron hopping model based on the Marcus-Hush theory and the segmental limited Brownian motion of redox-active sites (collectively known as the "diffusion-cooperative" model).[19] CRPs structurally hybridize π-conjugation and redox centers. Electrons can "hop" across isoenergetic redox centers when the electron densities are continuous. Therefore, charge transfer across CRPs is potentially a combination of mechanisms, including collision-based electron self-exchange, intra- and inter-chain charge hopping, and simultaneous electro-inactive counterion migration to maintain charge neutrality. The sub-second scale charge transfer mechanism, and therefore the conductivity, of *branched CRPs* are typically ascribed to non-thermally activated (*ipso facto*, not redox rate-limiting) polaron hopping mechanisms.[20 21]

Overall, structure-dependent charge transfer mechanisms in CRPs are not well understood relative to CPs and RPs, especially in the context of bioelectrocatalysis. Mechanistic understanding of charge transfer in electroactive polymers is instrumental in designing effective biotic-abiotic interfaces of bioelectrocatalytic hybrids. For instance, the influence of the deposition strategy of redox mediating polymers on bioelectrocatalytic performance directly correlates to the polymeric structure and, therefore, the charge propagation mechanisms through biohybrids. Zahn et al. have observed that apparent electron diffusion coefficients (D_{app}) of "*mixed*" multilayers of branched polyelectrolytes are distinctly higher than their "*layer-by-layer*" depositions, due to higher interactions between different polyelectrolytes leading to higher apparent diffusional exchange of electrons (i.e., interdiffusion) in the former.[22] Grattieri et al. observed that "*mixed*" deposition (homogenous mixture of electroactive materials including polymer and biocatalysts) of a *branched RP* and the purple bacterium *Rhodobactor capsulatus* recorded superior photobioelectrocatalytic performance over the *"layered"* (deposition of separate sequential layers of electroactive materials), due to the pronounced ability of partially mobile, peripheral redox centers in the polymer to extract electrons from the biocatalyst.[23] Conversely, we have previously reported that the "*layered"* deposition of *unbranched CRP*, polydihydroxyaniline (PDHA), achieves significantly superior biophotovoltaic currents (4.2 × increment) compared to the "*mixed*" (2.4 × increment) counterpart in photobioelectrocatalytic biohybrids of PDHA and plant chloroplasts.[2] The "*layered"* deposition resulted in the highest photocurrent density recorded with intact chloroplasts during photobioelectrocatalysis ($-48 \pm 3\ \mu A\ cm^{-2}$), when the biohybrids were supplemented with the diffusible redox mediator 2,6-dichlorobenzoquinone.

The *unbranched CRP* structure of PDHA molecularly couples redox centers and π-conjugation, theoretically merging redox conversions and conductance across the polymer. Thereby, while PDHA is a superior charge transfer conduit to electrochemically-wire intact chloroplasts to electrode surfaces during photobioelectrocatalysis, its redox mediating functionality can clearly be further optimized by modulating the deposition strategy of polymer and biocatalyst. In this study, we electrokinetically assess the charge transfer mechanisms in "*mixed"* and "*layered"* PDHA-chloroplast biohybrid architectures during the conversion of light to electrical energy, to rationalize the contrasting photobioelectrocatalytic performances previously reported. We elevate the existing understanding of incisive modulation in biohybrid designs and depositions to optimize their photobioelectrocatalytic efficiency.

Experimental

Chemicals and materials.—Ammonium persulfate (>98% purity) was purchased from J. T Baker chemicals. Ethylenediaminetetraacetic acid (EDTA), ethylene glycol diglycidyl ether (EGDGE) (>99.5% purity), glycerol, 4-(2-hydroxyethyl)piperazine-1-ethanesulfonic acid (HEPES) (>99.5% purity), 3-(n-morpholino)propanesulfonic acid (MOPS) (>99.5% purity), magnesium chloride (>99% purity), potassium hydroxide (>99% purity), salicylic acid (>99% purity), sodium chloride (>99% purity), sorbitol (99.5% purity), 2,2,6,6-tetramethylpiperidine 1-oxyl (TEMPO) (98% purity) were purchased from Sigma-Aldrich. Chemicals were analytical or research-grade and were used as received without further purification unless specified otherwise. Ultrapure type 1 Milli-Q water (18 $M\Omega\ cm^{-1}$) was used in all synthetic and electrochemical experiments. A pycnometer (5 ± 0.0001 ml) was purchased from CarlRoth labware. Nunc™ Lab-Tek™ Chambered Coverglass in the 8-well format (catalog number 155411PK) was purchased from ThermoFisher Scientific. Spectrum™ Spectra/Por™ 6 pre-wetted standard RC Dialysis Tubing, 6–80 kD MWCO was purchased from Fischer Scientific. The conducting redox polymer PDHA, wherein quinone and aniline have redox potentials of −0.032 and −0.239 V vs SCE, respectively, was synthesized and characterized as previously reported.[2,24,25] Intact chloroplasts were isolated from Spinach (*Spinacia oleracea*) into chloroplast isolation buffer (CIB, pH 7.8) as previously reported and stored at −80 °C after adjusting the chlorophyll concentration to $1\ mg\ ml^{-1}$ with 10% glycerol stock.

Inducing detectable fluorescence in PDHA.—Fluorescence was induced in PDHA (Scheme S1), adapting a previous report (Kargiwar et al.) on inducing fluorescence in polyaniline.[26] A suspension of PDHA (0.2 M, assuming $\sim 136.11\ g\ mol^{-1}$ molecular weight) and salicylic acid (0.1 M) in milli-Q water (12.5 ml) was stirred at room temperature for 2 h. An aqueous ammonium persulfate solution (0.2 M, 6.25 ml) was added dropwise to the suspension and left to stir overnight. The resulting black PDHA precipitate was washed with water, and methanol, dried under vacuum for 6 h and stored under N_2.

Working electrode preparation.—A geometric surface area of 1 cm^2 on carbon paper electrodes (AvCarb MGL 190, Fuel Cell Store, College Station, TX) was used to drop cast depositions of each working electrode. The *solely-PDHA* electrodes comprised the PDHA suspension (30 μl, $10\ mg\ ml^{-1}$) and EGDGE binder (2.86 μl, 10% *v/v*). The *solely-chloroplast* electrodes comprised the chloroplasts suspension (30 μl, $1\ mg\ ml^{-1}$) and EGDGE (2.86 μl, 10% v/v). The deposition material for *"mixed"* and *"layered"* biohybrids were the PDHA suspension (30 μl, $10\ mg\ ml^{-1}$), chloroplasts suspension (30 μl, $1\ mg\ ml^{-1}$), and EGDGE (2.86 μl, 10% *v/v*). After dropcasting depositions, electrodes were dried under N_2 inside a desiccator in the dark for 30 min. In the "*layered*" biohybrid, the chloroplast suspension was drop cast on the electrode after the solution of PDHA and EGDGE. Each of the two layers was dried under N_2 for 15 min.

Working electrodes for the rotating disk electrode (RDE) experiments were prepared on rotating electrode shafts with E3 series fixed-disk glassy carbon RDE tips, 5.0 mm disk OD, by Pine Research. The electrodes were polished with 0.05 μm alumina slurry and rinsed thoroughly with Milli-Q water before each use. Due to the small surface area of the electrode, the deposition quantities of each constituent in solely-PDHA, "*mixed*," and "*layered*" electrodes were

halved from the quantities used on carbon paper. Calculation adjustments were made accordingly. A standard RC Dialysis Tubing (6–80 kD MWCO), halved to form a dialysis membrane and an O-ring were used to cover the adlayer on the glassy carbon electrode.

Imaging depositions by confocal fluorescence microscopy.— The fluorescence induced PDHA and chloroplast depositions on chambered glass coverslips were dried under N_2 for 30 min. Each well was introduced 500 μl of MOPS buffer, to recreate electrolyte-induced swelling. All confocal fluorescence microscopy images in this study were acquired with a Zeiss LSM 880 Airyscan and a 63 × oil-immersion objective with 1.4 numerical aperture (N.A.) and 2KX2K resolution for three channels (green, red, and transmittance). The chambered glass coverslip systems were positioned and mounted on the microscope stage at a 180-degree angle with respect to the microscope oil-immersion objective. For samples containing chloroplast, the autofluorescence of chlorophyll was utilized for visualization of chloroplast structures. Laser lines with wavelengths of 488 nm and 575 nm were used to measure fluorescence. All images were captured using Zen image-capture software. All data were stored as 2048- by 2048-pixel (67.48- by 67.48-μm pixel size) 8-bit z-stack images. Confocal fluorescence microscopy image stacks (three-dimensional (3D) slice images) were acquired at 0.5 μm steps (in the z-axis direction) and these stack images were used to obtain the average thickness values for each sample. All images were processed with Fiji Software and ImageJ Software.

Determining PDHA concentration based on unpaired electron density.—The density of solid PDHA was determined utilizing a pycnometer via hydrostatic weighing and the Archimedes' principle.[27]

Electron paramagnetic spectroscopy (EPR).—EPR experiments were performed on a Bruker EMX X-band rectangular cavity CW instrument. All samples were measured at room temperature (21 °C ± 4 °C). The instrument was calibrated for quantitative EPR measurements using TEMPO to construct a standard calibration curve. Samples were prepared in triplicate, weighed, and transferred to 5 mm quartz EPR tubes. Special care was taken to reduce static electricity in the weighing environment for error minimization with the aid of an alpha ionizing cartridge. The spin density of PDHA was calculated using the sample mass, powder density, and Avogadro's number (Eqs. S1–S2).

Electrochemical setup and measurements.—Cyclic voltammetry (CV), double potential step chronoamperometry (DPSCA), and electrochemical impedance spectroscopy (EIS) were performed with a CHI 660 E potentiostat, using a standard three-electrode cell configuration. All potentials are reported vs saturated calomel reference electrode (SCE). A Pt mesh was used as the counter electrode. MOPS buffer (7.0 pH) containing 10 mM $MgCl_2$ was used as the electrolyte. Inert anoxic conditions were maintained by bubbling N_2 through and over the systems before and during all experiments. A Dolan-Jenner Fiber-Lite lamp (Model 190–1 quartz-halogen illumination system with an optical light guide providing a light intensity of 76 mW cm^{-2}) was used for illumination conditions. The averaged fourth scan is shown for all the reported cyclic voltammograms to allow stabilization of the system. During DPSCA, starting potential was stepped from 0 to +0.3 V, followed by −0.3 V. Each pulse width was 20 s. All electrochemical data are reported according to polarographic notation, where a negative current represents oxidative reactions. Electrochemical experiments at 35 °C ± 4 °C and 50 °C ± 4 °C were conducted in thermostatic water baths.

.—Amperometry experiments under increasing temperature were conducted individually under light and dark conditions, using the electrochemical setup previously used for amperometry (−0.3 V). The initial 900 s of the amperometry scans were maintained under dark to allow stabilization of the system. The electrochemical cells for amperometry scans under "light" were subsequently illuminated, while the scans under "dark" were continuedly kept in the dark. The initial electrolyte temperature of each system was maintained at 21 ° C ± 4 °C. A Corning ceramic top hotplate (Thermal scientific, Texas) at heat setting 4 was used to gradually heat the system. A temperature probe immersed in the electrolyte at a level with the working electrode was used to record the temperature at 30 s intervals till the final temperature was 45 °C. The current density increments under varying temperatures reported in Fig. 5 were calculated by subtracting the current density at the 900th s of the amperometry trace from the subsequent anodic currents in the time scale. The x-axes of the plots were constructed by correlating the recorded temperature to the time of each amperometry curve.

.—Rotating disk experiments (RDE) were performed on an RRDE-3A rotating disk electrode instrument (catalog number A-012180). The electrochemical cell was placed on a glass slide to illuminate the inverted RDE shaft surface by the fiber-lite light source.

.—Electrochemical impedance spectroscopy (EIS) data was obtained using the AC impedance technique in the CHI 660 E potentiostat for working electrodes fabricated on carbon paper and under illumination. The 10^6-10^1 Hz frequency range and 0.005 V amplitude were used. The open-circuit potential of the system was tested with time before and after acquiring each AC impedance spectrum. Equivalent circuits for the AC impedance spectra were

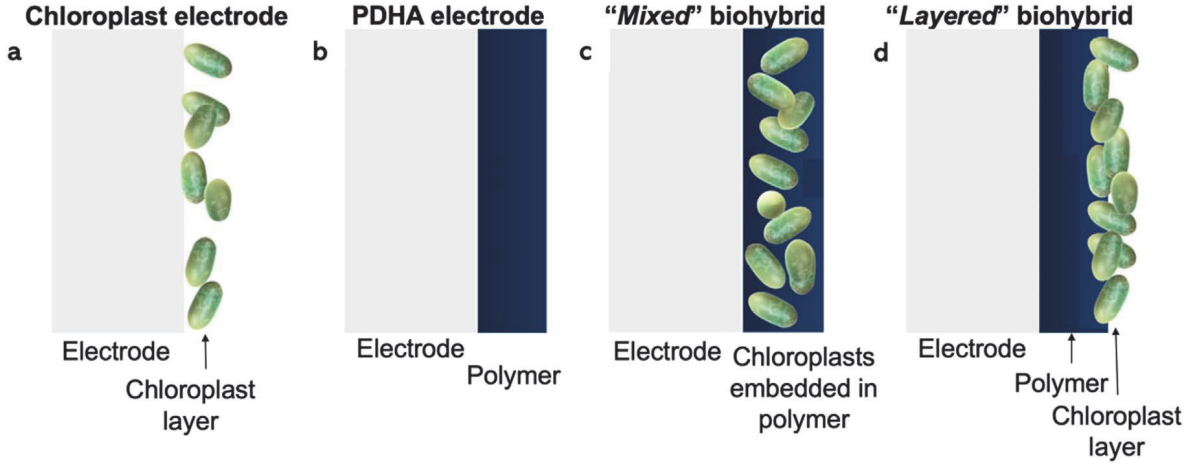

Scheme 1. Schematic diagram of (a) chloroplast electrodes, (b) PDHA electrodes, (c) "*mixed*," and (d) "*layered*" depositions of PDHA on carbon electrodes.

modeled using the CHI 660 E software. At least three independent replicate experiments were performed for all the electrochemical characterizations, and the average currents are reported in the manuscript along with corresponding standard errors.

Results and Discussion

The two main goals of this work are to experimentally understand the dominating mechanism of electron transport in PDHA-chloroplast biohybrids (i.e., whether the PDHA is acting primarily as a conducting polymer (CP) or a redox polymer (RP) in the biohybrids) and to use that understanding to modulate different deposition strategies of CRPs on electrodes to maximize photobioelectrocatalysis. We investigated a solely-chloroplast and a solely-PDHA electrode, and "*mixed*" and *"layered"* geometry biohybrids (Scheme 1).

Imaging the electrode depositions.—Confocal Raman and confocal fluorescence microscopy were used to image the depositions (Figs. S1, S3 (available online at stacks.iop.org/JES/169/085501/mmedia)). Weak intrinsic fluorescence and intense color of PDHA limit the use of microscopic techniques to probe the morphologies of the depositions.[2] (Fig. S2). Conventional "fluorescence tagging" techniques utilized in confocal fluorescence microscopy can sterically distort the distribution of electroactive material in each deposition.[8] Therefore, dopant p-type salicylic acid was used to form a donor-acceptor conjugated π-system with the imine centers in PDHA (Scheme S1), reducing the gap between the valence and conductance bands.[28] The fluorescence quantum yield and emission wavelength of the sample increase, synthetically inducing fluorescence in PDHA,[29] detectable by confocal fluorescence microscopy (Figs. 1, S3). Confocal fluorescence microscopy images reflect the expected "*mixed*" and "*layered*" depositions depicted in Scheme 1.

A significant outcome of the "*layered*" deposition is the lowered obstruction by the intense blue-black PDHA for panchromatic light to reach chloroplasts, which maximizes electrocatalytically significant light absorption, compared to the *"mixed"* deposition. We hypothesize that the collective photobioelectrocatalytic charge transfer across the electrically conducting "*layer"* of PDHA between electron source (i.e., photobiocatalyst) and sink (i.e., electrode) is more facile compared to across the "*mixed"* counterpart.

Based on the assumption that the depositions approximate a rectangular cuboid shape on porous, tortuous carbon paper upon swelling by electrolyte, average thicknesses and radii of the drop cast films obtained from confocal fluorescence microscopy images, and spin densities were utilized to calculate the PDHA concentration in each electrode (Table SI). PDHA concentrations of the solely-PDHA electrode and the "*mixed"* biohybrid were 5.23 (±1) $\times$ 10^{-5} mol cm^{-3}, 0.674 (± 0.01) $\times$ 10^{-5} mol cm$^{-3,}$ respectively, while the PDHA layer in the "*layered"* biohybrid recorded 1.56 (± 0.07) $\times$ 10^{-5} mol cm^{-3}. The surface coverage (Γ) of adsorbed PDHA after deposition on each electrode was quantified using cyclic voltammetry in the absence of photobioelectrocatalysis (Figs. S4–S6, Table SII). The Γ values for the solely-PDHA electrode, "*mixed"* and "*layered"* biohybrids were 1.29 (±0.14) $\times$ 10^{-11}, 7.18 (±0.96) $\times$ 10^{-12}, and 6.66 (±0.03) $\times$ 10^{-12} mol cm^{-2}, respectively.

Surface adhesion of the bioelectrode formulations.—Unlike the transparent and colorless borosilicate glass covers used for film deposition in confocal fluorescence microscopy, the opaque, porous carbon Toray paper surfaces used in photobioelectrocatalytic cells introduce a significant degree of tortuosity to the biohybrid electrodes and warp the depositions layers. The electroactive volume of the bioelectrodes constitutes the porous carbon electrode surface, PDHA, chloroplasts, binder, and the voids in between imbibing ion-conducting electrolytes. Cross-sectional environmental SEM was used to image the electrodes "swollen" with electrolyte, without the aid of conductive coatings (Figs. S7, Table SIII). Laser profilometry was used to image the thickness variations of the electroactive material deposited on carbon paper qualitatively (Figure S8–S11).

The ability of the PDHA in biohybrids to function as immobilization matrices for chloroplasts was compared by measuring the absorbance of chloroplasts suspended in the electrolyte after 1500 s amperometry cycles, using an Evolution 260 Bio UV−visible spectrophotometer (Thermo Scientific, Waltham, MA) at 652 nm (Table SIV). The electrolyte from the electrochemical cell with the solely-chloroplast working electrode recorded the highest absorbance at 652 nm, while the electrochemical cell with the "*layered*" deposition recorded the lowest. The higher absorbance signal corresponds to higher quantities of chloroplasts that have disintegrated from the deposition into the electrolyte during electrochemical cycling.

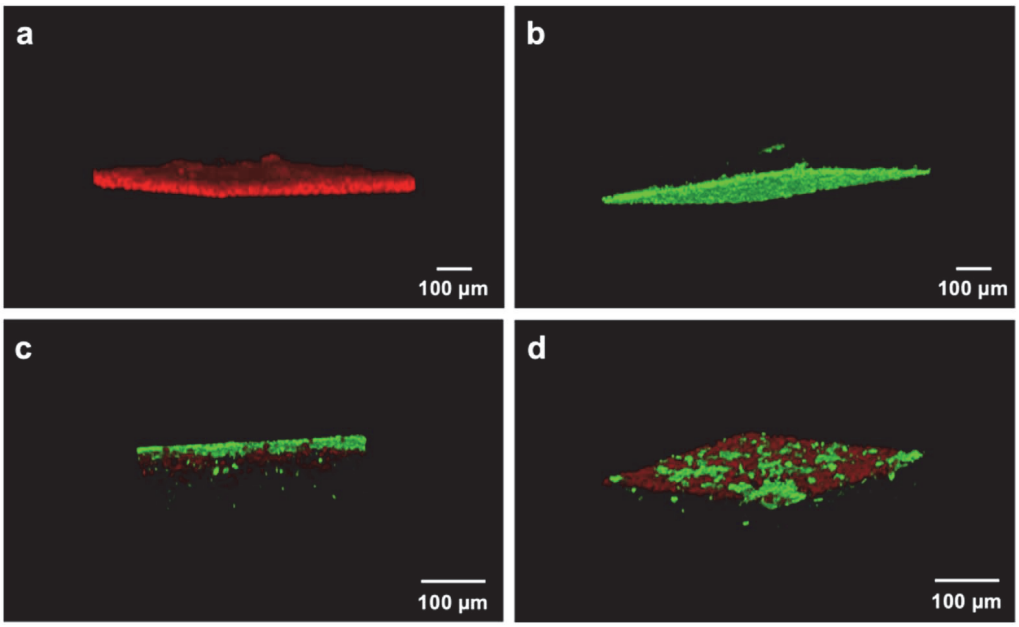

Figure 1. Confocal fluorescence microscopy three-dimensional (3D) image stacks of electrodes with (a) chloroplast, (b) salicylic acid doped PDHA, (c) "*layered*," and (d) "*mixed"* biohybrid depositions. Chloroplasts are shown in red fluorescence signals and doped PDHA as green fluorescence.

PDHA as a conduit for charge carriers.—The substantially different photobioelectrocatalytic currents reported for solely-chloroplast electrodes, "*mixed*" and "*layered*" biohybrids (*vide supra*) are a manifestation of differential (i) transfer of catalytic electron flux from chloroplasts to redox mediating polymer, (ii) the diffusion of the catalytic electron flux across bioelectrodes, (iii) the concomitant counterion migration to maintain charge neutrality on polymer, (iv) mass transfer of reactants, and (v) heterogeneous electron transfer to the electrode.[14,30] The nature of electrolyte-electrode interactions, electrostatic interactions, inhomogeneity of the redox polymer and chloroplasts, and lateral interactions that underscore these inhomogeneities influence the charge transfer processes in each biohybrid.[31] Considering that in the PDHA-chloroplast photobioelectrocatalytic systems in question: (i) the oxidizing anodic substrate is water at the chloroplasts, (ii) the electrolyte is aqueous, and (iii) all biomembranes imbibe a considerable volume of water, the mass transfer of water as the substrate is assumed to be a non-limiting step. Considering photosynthetic events in chloroplasts such as photon absorption, charge separation, fluorescence, and electron transfer reactions of physicochemical significance occur in a timescale of 10^{-15}–1 s,[32] charge transfer from photobiocatalyst to polymer is also assumed to be a non-limiting step.

Apparent electron diffusion coefficient (D_{app}).—Considering that PDHA is a conducting redox polymer (CRP), it could either behave primarily as a CP or a RP in the biohybrid electrodes. We first evaluated this fundamental question with traditional electroanalytical tools.

The diffusion coefficient (D) quantifies the rate of transport as a ratio of flux density to the concentration gradient during diffusion, according to Fick's law.[33] The D values at the modified electrode surfaces are typically quantified using a diffusible analyte,[34,35] or a specific standard redox mediator.[36,37] If the electroactive species is surface-immobilized, such as the PDHA electrodes, Fick's law is applied to the electrolytically generated concentration gradient of the donor (electron) and acceptor (hole) sites during "diffusion-like" electron transfer by the respective redox reaction across the polymer.[31,38,39] This interpretation of the apparent electron diffusion coefficient (D_{app}) necessitates that the rate-limiting step during the overall mechanism is charge transfer through the polymer or polymer-catalyst film, and not an auxiliary process.[38] Quantifying the concentration of redox-active species (C), that forms the aforementioned electron gradient across the CRP-biocatalyst biohybrid interface, in order to determine D_{app} is experimentally problematic. Therefore, we have combined transient and steady-state concentration gradient measurements (respectively analyzed by Cottrell and Koutecký-Levich models) to determine the concentrations, and D_{app} of each electrode (Table I). S*teady-state concentration gradients* are linear and have a constant flux, as opposed to *transient concentration gradients*, the tandem use of which will prevent the underestimation of D_{app} due to overgeneralization of the contribution by counterion migration to the overall charge transfer mechanism in the electrodes during photobioelectrocatalysis.[13 35,40] Supplementary compounded unit of $|CD_{app}{}^{1/2}|$ for each electrode is also provided (Table I), which is a quantitative parameter of the rate of electron diffusion through RPs, independent of (i) varying electroactive material concentrations as a function of distance from the electrode surface, and (ii) unaccounted aggregation of electroactive material as a function of electrolyte pH, ionic strength, etc., which in turn influence diffusion-like charge transfer.

Cottrell method.—Cottrell analysis of DPSCA data has been utilized to determine the catalytic rate constant and the D of either irreversible transformations of diffusible analytes,[35,41] reversible reactions of diffusible redox mediators,[42,43] or the rate of electron transfer to redox-polymer modified electrode surfaces.[38,43,44]

$$i_d(t) = \frac{nFA(D_{app})^{1/2}C}{\pi^{1/2}t^{1/2}} \quad [1]$$

where i_d is the current, and t is the time, n is the number of electrons transferred, F is the Faraday constant, D_{app} is the apparent electron diffusion coefficient, and C is the concentration of the redox-active species.

The potential steps in DPSCA were selected considering the applied potential to extract recorded biophotovoltaic performances during amperometry experiments (−0.3 V vs SCE). The initial 10–20 ms time window at the beginning of the second sweep of DPSCA was used for the Cottrell analysis (Eq. 1), as is typical for redox polymers. The slope of each plot of current density vs reciprocal square root of time (Fig. 2) was used to quantify $|CD_{app}{}^{1/2}|$ (Table I). The non-zero intercepts of these Cottrell plots were attributed to the substantial capacitive currents of PDHA films at the electrode-electrolyte interface. However, Forster et al. attributed a similar baseline current in Cottrell plots for an Osmium-based branched RP to the migration effects of perchlorate-based electrolytes.[44]

The current-time response of the Cottrell equation is based on the assumptions that (i) the potential step is large enough to induce an instantaneous change in surface concentration, (ii) the electrode is planar (semi-infinite linear diffusion), and (iii) the absence of convective disruptions.[45] Biohybrid electrodes under investigation are porous, heterogeneous, and semi-infinite conditions are poorly maintained, especially at higher temperatures where turbulent convections are introduced to the electrochemical cell, overestimating the $CD_{app}{}^{1/2}$. Intuitively, the *cell time constants* for the three electrodes would be different due to the differences in double-layer capacitances (C_d) and uncompensated solution resistances (R_u) among the PDHA, and biohybrid electrode formulations, obscuring the effective Faradaic currents applicable for analysis.[45]

Koutecký-Levich method.—Steady-state diffusion conditions forgo the concentration and time dependency (i.e., decouple macroscopic counterion migration from electron transfer) observed in transient $CD_{app}{}^{1/2}$ measurements from quiescent solutions, significantly deconvoluting the analysis of charge transfer across modified electrode surfaces in the former.[13,45]

The RDE data for the solely-PDHA, "*mixed*" and "*layered*" electrodes investigated in this study deviate from the characteristic sigmoidal voltammetry shape (Fig. S12). A dialysis membrane is used to secure the physisorbed adlayer on the electrodes against the centrifugal force generated on the inverted surface during rapid rotation. While the membrane is conducive to efficient proton and counterion migration, its presence significantly alters the hydrodynamic boundary layer of the RDE. The anodic and cathodic cyclic voltammogram halves for the non-catalytic electron transfer in the solely-PDHA electrode do not overlap, probably due to the uneven and thick deposition of polymer, which increases the diffusion length inside the hydrodynamic layer. The anodic and cathodic cyclic voltammogram halves of the two biohybrid electrodes also do not overlap because of the catalytic and sluggish nature of the electron transfer through each thick uneven biohybrid deposition.

The Levich flux ($0.62\,C\,D^{2/3}\,\nu^{-1/6}\,\omega^{1/2}$) estimated by the Levich equation (Eq. 2) projects entirely mass transfer-controlled, steady-state conditions. Alternatively, the Koutecký-Levich equation (Eq. 3) encompasses kinetic limitations on the electrochemical system by quantifying a current in the theoretical absence of any mass transfer effects (i_K at $\omega = \infty$).

$$i_L = 0.62nFACD_{app}^{2/3}\nu^{-1/6}\omega^{1/2} \quad [2]$$

Table I. Averaged $CD_{app}^{1/2}$ values for the solely-PDHA electrode, "*mixed*," and "*layered*" biohybrid electrodes, at room temperature (21 °C ± 4 °C), 35 ± 4 °C, and 50 ± 4 °C, based on the Cottrell equation. Averaged $CD_{app}^{2/3}$ values for the solely-PDHA electrode, "*mixed*," and "*layered*" biohybrid electrodes at room temperature (21 °C ± 4 °C) based on the Koutecký-Levich equation. The concentration of the monomers in electrical communication within the polymer-modified electrodes is determined by incorporating Cottrell- Koutecký-Levich models. The D_{app} values of each deposition are based on (i) conjoining the two models, (ii) pairing the Koutecký-Levich analysis to PDHA concentrations obtained via EPR, and (iii) pairing the Cottrell analysis to PDHA concentrations obtained via EPR.

Electrode	Average $CD_{app}^{1/2}$ by Cottrell Method ($\times 10^{-9}$ mol cm^{-2} s$^{-1/2}$)			Average $CD^{2/3}$ by Koutecky-Levich Method ($\times 10^{-11}$ mol cm$^{-8/3}$ s$^{-2/3}$)	Concentration of PDHA monomers in electrical communication by Cottrell and Koutecky-Levich Methods (mol cm^{-3})	D_{app} (cm^2 s^{-1}) by the Cottrell Model		
	21 °C	**35** °C	**50** °C	**21** °C	**21** °C	**21** °C	**35** °C	**50** °C
PDHA electrode	1.33	1.50	4.84	2.08	3.50×10^{-4}	1.45×10^{-11}	2.08×10^{-10}	1.91×10^{-10}
	(±0.09)	(±0.06)	(±0.06)	(±0.23)		(±0.20)	(±0.02)	(±0.05)
"*Mixed*" biohybrid	0.736	1.11	3.07	2.08	3.25×10^{-5}	5.14×10^{-10}	1.17×10^{-9}	8.94×10^{-9}
	(±0.045)	(±0.03)	(±0.54)	(±0.70)		(±0.61)	(±0.07)	(±0.34)
"*Layered*" biohybrid	0.683	1.18	2.75	33.4	5.84×10^{-9}	1.37×10^{-2}	4.06×10^{-2}	2.21×10^{-1}
	(±0.070)	(±0.18)	(±0.28)	(±17.1)		(±0.003)	(±0.01)	(±0.04)

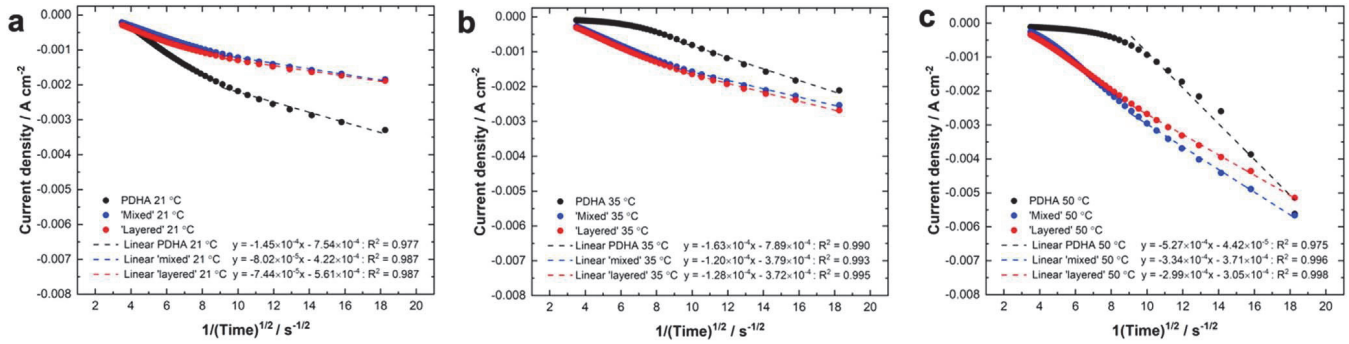

Figure 2. (a)–(c) Averaged Cottrell plots of current density vs reciprocal square root of time for solely-PDHA, "*mixed*," and "*layered*" biohybrid electrodes at: (a) room temperature 21 °C ± 4 °C, (b) 35 °C ± 4 °C, and (c) 50 °C ± 4 °C.

$$\frac{1}{i} = \frac{1}{i_L} + \frac{1}{i_K} = \frac{1}{0.620nFAD^{2/3}\nu^{-1/6}C}\omega^{-1/2} + \frac{1}{i_K} \quad [3]$$

where i_L is the limiting current, i_K is the limiting current at infinite rotation, ν is the scan rate, and ω is the rotation rate.

The positive Y-intercepts on the Koutecký-Levich plots (Fig. 3a) for the three electrodes indicate the charge transfer across the three depositions is kinetically limited by electron transfer. The i_K value for the solely-PDHA is an order of magnitude higher than the "*mixed*" and "*layered*" depositions, irrespective of the additional electron source provided by photobioelectrocatalysts in the biohybrids (Table SV). This observation is an indication that electron transfer from electrically insulating photobioelectrocatalysts to polymer, in addition to electron transport across the CRP, might be kinetically limiting. The i_K value for the solely-PDHA electrode is large enough for its corresponding Levich constant (i_L /C $\omega^{1/2}$) to remain constant (Fig. S13). Of the two biohybrids, the higher i_K of the "*layered*" corroborates a comparatively superior electron conduit.

The concentration of PDHA in electrical communication in polymer-modified electrodes and D_{app} values for the three electrodes were calculated by assimilating transient and steady-state condition measurements (Table I, Fig. 3b). As expected, the incorporation of biocatalysts decreases the concentration of redox species that can electronically connect to the electrode. This is dramatically observed with the "*layered*" deposition possibly due to its inhomogeneity wherein the first few micrometers of thickness are completely devoid of PDHA while the last few micrometers are saturated.

The D_{app} values for solely-PDHA electrodes increase with temperature (*vide supra*), reflective of Eq. 4 (Fig. 3b). The D_{app} values for analogous organic RPs are typically in the 10^{-8}–10^{-12} cm^2 s^{-1} range at room temperature.[1,22,46] Ergo, the D_{app} in the order of magnitudes of 10^{-11}–10^{-10} cm^2 s^{-1} obtained for PDHA in this study are reasonable estimations also reflective of its RP-characteristics.

$$D_{app} = D_0 e^{-\frac{E_a}{RT}} \quad [4]$$

where D_0 is the frequency factor, E_a is the activation energy, and R is the Gas constant.[44,47,48]

Both $CD_{app}{}^{1/2}$ and D_{app} values based on the Cottrell method for the biohybrids increased with temperature (Table I), indicative of increasing internal energy required to overcome activation barriers for electron transport (Eq. 4).

All the D_{app} estimations (Table I) increase in the ascending order of solely-PDHA electrode, "*mixed*," and "*layered*" depositions (Fig. 3b). Solely-PDHA electrode has the lowest value due to the lower electron flux without biocatalytic chloroplasts. The D_{app} for the "*layered*" deposition is quite high, but comparatively, the D_{app} for electrons in semiconducting silicon, determined by time-of-flight and noise measurements, is lower than 36 cm^2 s^{-1}.[49] This observation could either be a result of the architecture in the "*layered*" deposition that: (i) fixes the electron diffusion gradient across PDHA, between the electron source (chloroplasts) and sink (electrode surface), (ii) provides maximum light exposure to chloroplasts, (iii) better surface adhesion of the polymer layer, or due to a slight overestimation of D_{app} values owing to the uncertainty of the RDE data.

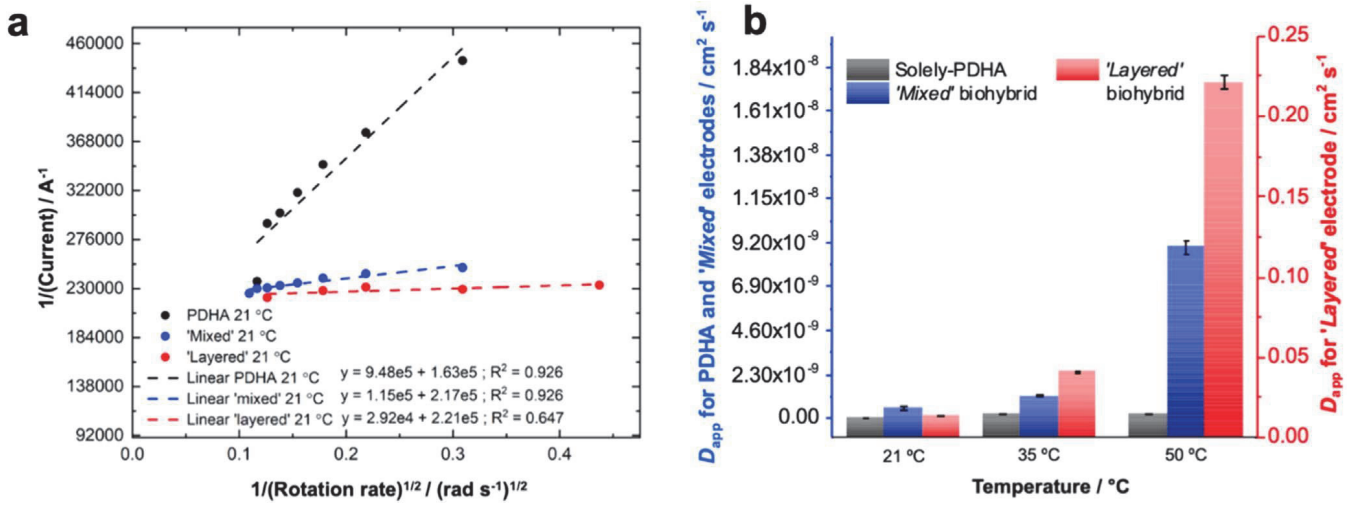

Figure 3. (a) Averaged Koutecký-Levich plots of reciprocal current vs reciprocal square root of rotation rate for solely-PDHA, "*mixed*," and "*layered*" biohybrid electrodes at room temperature, (b) D_{app} values for solely-PDHA, "*mixed*," and "*layered*" biohybrid electrodes calculated by assimilating transient and steady state measurements.

Majority charge carrier.—Sterby et al. have shown that the majority of the charge carriers in *branched CRPs* are polarons.[21] In order to determine the majority charge carrier across *unbranched CRP* PDHA, the unpaired electron density in PDHA corresponding to polarons was determined via EPR. One of the underlying assumptions was that all the recorded unpaired spin states are mobile and not stuck in trap states non-contributive to conductivity.

The EPR signal for PDHA showed a peak-to-peak linewidth of 13.3 G, a −1.14 ratio of peak amplitudes expected for the Dysonian line shape, and an average g-value estimation between 2.05 (Fig. 4b). The Dyson curve shape with broadening is common for conducting polymers like PANI.[50] The proximity of the *g*-value estimation to that of a free electron (2.0023)[51] suggests the resonance in the sample originates from the delocalized electrons in the π-conjugated polymeric system of P_z orbitals of C, O, N. Increased exposure to air increased the signal asymmetry and broadening, indicative of irreversible air oxidation and consequent stripping of electrons before shuttling across PDHA.[50] TEMPO standards were used to construct an EPR density calibration curve in order to determine the spin density of the PDHA powder samples. The powder density of PDHA obtained by hydrostatic weighing was 1.62 g cm^{-3}, and the determined spin density for PDHA was 1.54×10^{-4} mol cm^{-3} (9.29×10^{19} charges cm^{-3}). Assuming one polaron per monomeric unit (based on the unpaired electron density in the PDHA molecular structure. Figure 4), which is delocalized in and diffusing across the polymeric chain, the concentration of conducting monomers in PDHA was 1.04×10^{-4} mol cm^{-3}. The concentration of PDHA expected according to the stoichiometry of the synthetic reaction is 8.08×10^{-4} mol cm^{-3}. Comparatively, the effective concentration of PDHA in electrical communication via self-exchange across the solely-PDHA electrode computed by incorporating the Cottrell and Koutecký-Levich data (Table I) is over two-fold higher (3.50×10^{-4} mol cm^{-3}) than the estimated polaron concentration by EPR. This observation validates the assumption that the major charge carrier in PDHA is electrons, instead of polarons (i.e., PDHA functions more as an RP than a CP).

Activation parameters for the electron transport.—Monitoring D_{app} as a function of temperature is a facile approach to quantify the activation parameters pertaining to the electron transport across polymer depositions during photobioelectrocatalysis. However, the photobioelectrocatalytic activity of intact chloroplasts is temperature sensitive. The optimal temperature for photosynthetic proteins is approximately 20 °C. Intact chloroplasts heated at 35 °C for 10 min have shown down-regulated photosynthesis due to the inhibition of protein import and irreversible protein denaturation.[52] Growth temperatures above 32 °C disorient the chloroplast lamellar system and alter the fluidity of membrane lipids and conformations of membrane proteins, reducing photoactivity.[53] Therefore, the suitable temperature window to investigate the electron transport mechanism is limited.

Current density increments obtained from amperometric *i–t* curves under varying temperatures, and light/dark conditions for the three electrodes (Fig. 5) indicate that: (i) the presence of PDHA increases current compared to solely-chloroplast electrodes, and (ii) the "*layered*" deposition elicits significantly higher currents than the "*mixed*" at all temperatures. Electron hopping through CRPs is a thermally activated process and increased random thermal motion surges collision-based electron tunneling. The solely-PDHA electrodes recorded: (i) consistent current increments with temperature, (ii) irrespective of light/dark conditions, possibly due to the thermoelectric properties of PDHA.[54] Highly ordered and doped PANIs have reported benchmark thermoelectric properties among CPs. However, the amorphous nature of the synthesized PDHA attenuates its potential thermoelectric properties.[48]

Arrhenius equation.—The D_{app}-based form (Eq. 4) of the Arrhenius equation is used to determine the activation energies (E_a) and frequency factors (D_0) for "diffusion-like" electron transfer across each of the biohybrid depositions (Fig. 6b).[44,47] According to the DPSCA data under varying temperatures (Table II), E_a values for the biohybrids were higher, as they involve a photobioelectrocatalytic transformation in addition to the electron diffusion accounted in the solely-PDHA electrode. The minimum energy barrier for

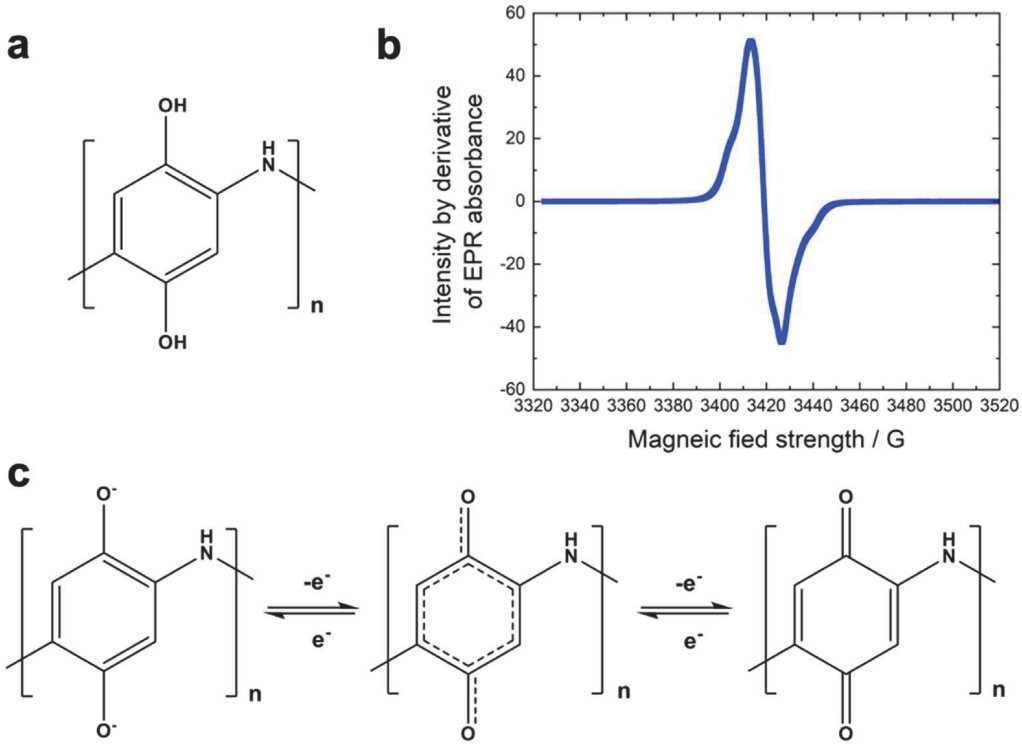

Figure 4. (a) Monomeric PDHA unit, (b) EPR signal for PDHA under air, (c) redox mechanism for PDHA depicted on the monomeric unit.[24]

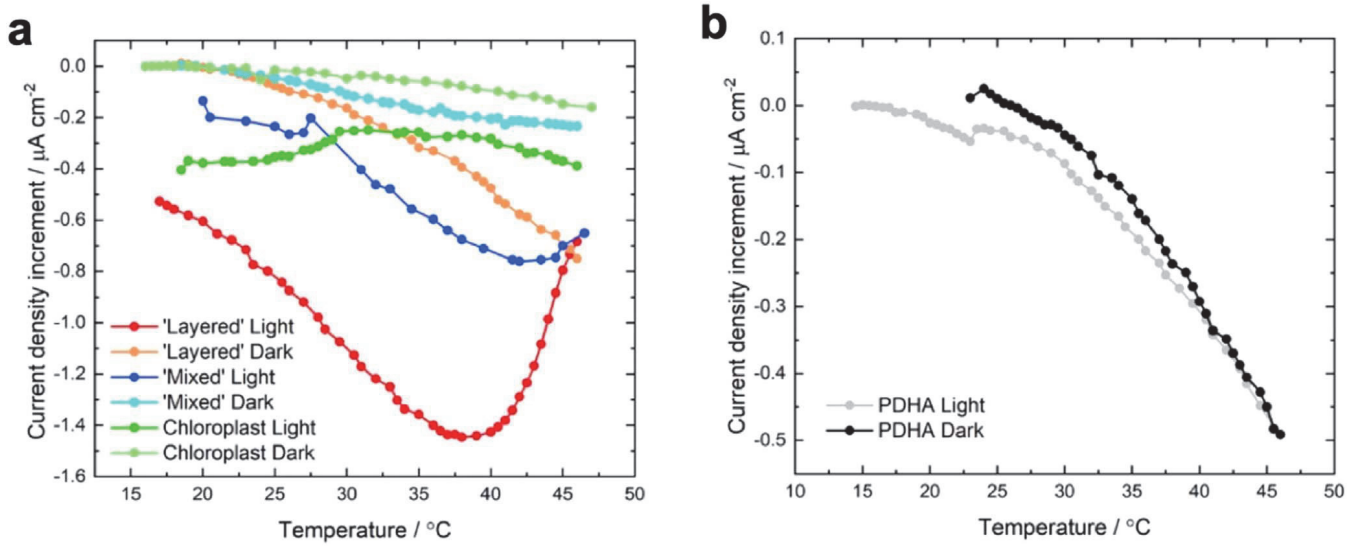

Figure 5. Representative current density increments under varying temperature and Light/Dark conditions for: (a) "*Layered*," "*mixed*" biohybrids and solely-chloroplast electrodes, (b) solely-PDHA electrodes.

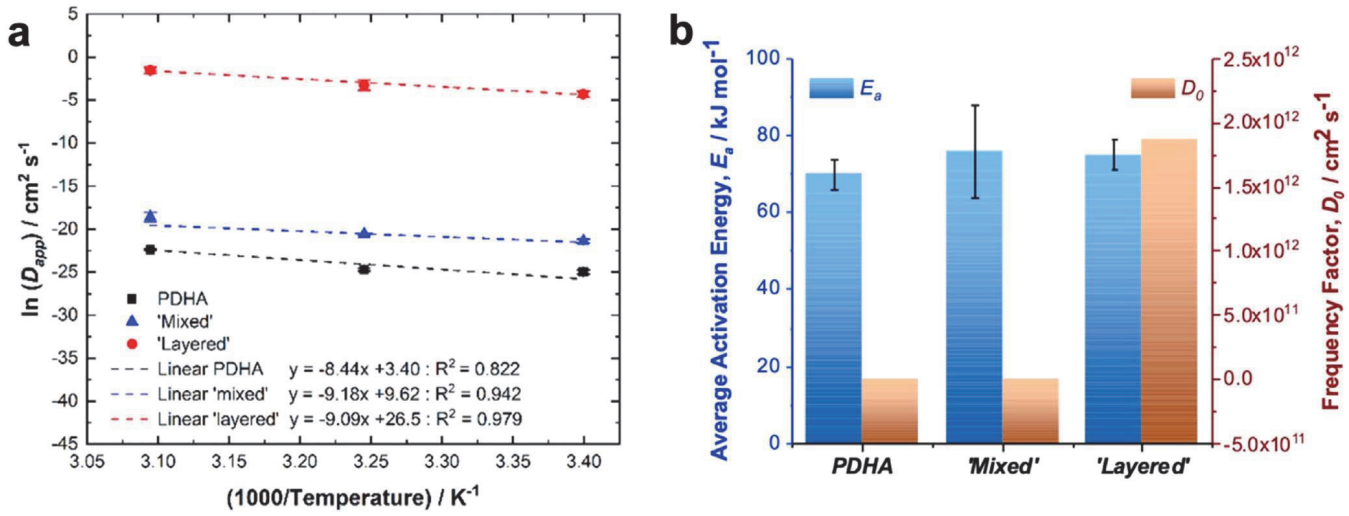

Figure 6. (a) Arrhenius plots of peak current vs scan rate for solely-PDHA, "*layered*," and "*mixed*" biohybrid electrodes, based on the Cottrell model, (b) Graphical representation of the average activation energy (E_a) and frequency factor (D_0) for "diffusion-like" electron transfer across solely-PDHA, "*layered*," and "*mixed*" biohybrid electrodes.

Table II. Averaged activation parameter (e.g., activation energy, frequency factor, entropy, enthalpy) for charge transfer through the solely-PDHA electrode, "*mixed*," and "*layered*" biohybrids, based on the Cottrell model.

Electrode	Average E_a (kJ mol^{-1})	Average D_0 (cm^2 s^{-1})	$\Delta S^{\neq}$(J K^{-1} mol^{-1})	$H^{\neq}$(kJ mol^{-1})
PDHA electrode	70 (±4)	2.19×10^2	21 °C: (70.7 ± 13.9)	21 °C: (67.8 ± 4.3)
			35 °C: (70.3 ± 13.9)	35 °C: (67.7 ± 4.3)
			50 °C: (69.9 ± 13.9)	50 °C: (67.5 4.3)
"*Mixed*" biohybrid	76 (±12)	7.65×10^7	21 °C: (122.4 ± 40.3)	21 °C: (73.9 ± 12.2)
			35 °C: (122.0 ± 40.3)	35 °C: (73.8 12.2)
			50 °C: (121.6 ± 40.3)	50 °C: (73.7 ± 12.2)
"*Layered*" biohybrid	75 (±4)	1.87×10^{12}	21 °C: (270.2 ± 12.3)	21 °C: (73.2 ± 3.6)
			35 °C: (270.0 ± 12.3)	35 °C: (73.0 ± 3.6)
			50 °C: (269.4 ± 12.3)	50 °C: (72.9 ± 3.6)

electron transfer across the "*layered*" biohybrid was lower than the "*mixed*" counterpart.

The D_0 analogous to the pre-exponential factor representing the frequency of molecular collisions is a manifestation of the steric contribution of the depositions for collisions and charge transfer. The D_0 values increase in the order of PDHA, "*mixed*" and "*layered*," reflective of the disparate PDHA distributions in each deposition, and respective observed currents. PDHA has the lowest

D_0 due to the absence of photocatalytic currents. The "*layered*" deposition recorded a remarkably high D_0 due to the localization of PDHA and chloroplasts into layers of electron source and sink, conducive for electron transfer. The lower D_0 in "*mixed*" biohybrids is also indicative of the longer distances between neighboring PDHA for electron tunneling or hopping, due to the presence of interspersed electrically-insulating chloroplasts.[55]

Eyring equation.—The D_0 of the Arrhenius equation has been derived through the Eyring equation based on a statistical mechanical justification for the reaction rate of a chemical mixture as a function of temperature (Eq. 5).[44,56]

$$D_0 = e\delta^2\left(\frac{k_B T}{h}\right)e\left(\frac{\Delta S^{\neq}}{R}\right) \quad [5]$$

where δ is the mean separation between the redox sites in PDHA, k_B is Boltzmann's constant, h is Planck's constant, and $S^{\neq}$ is the activation entropy for charge transfer.

The δ for PDHA is the distance between two adjacent quinones, which corresponds to two benzene ring centers on either side of imine N in the polymer chain. Assuming the bond length variations due to the conjugation of quinones in the polyaniline structure of PDHA are negligible, well-documented theoretical calculations for bond lengths of PANI were used to estimate δ for PDHA(~1.91 Å).[57] Activation entropy ($\Delta S^{\neq}$) for electron transfer in each electrode during photobioelectrocatalysis was computed utilizing Eq. 5 (Table II). The contribution by the electrolyte to $\Delta S^{\neq}$ was considered constant for all three electrodes. There are several alternative precedents for the interpretation of entropy data during electron transfer. Daum et al.[55] and Sun et al.[56] have stated that large positive activation entropies imply segmental mobility-limited charge transfer, and negative entropies imply counterion transport-limited charge transfer. Ergo, the positive $\Delta S^{\neq}$ values in our study indicate that sluggish electron hopping/tunneling is the rate-limiting step in electron transport in the three electrodes. Considering that redox conversions of quinones are typically proton-coupled electron transfers (Fig. 4c) and the electrolyte used is aqueous, counterion migration is less likely to be the rate-limiting step compared to electron tunneling/hopping in this case. The $\Delta S^{\neq}$ values for the two biohybrids were more positive than the solely-PDHA electrode as they encapsulate the activation entropy for electron transfer across each deposition in the presence of an extrinsic electron influx generated by photobioelectrocatalysis, increasing the system disorder. The substantially more positive entropies of the "*layered*" deposition than the other two electrodes are ascribed to its higher disorder caused by the presumed faster and larger electron flux between chloroplasts and electrode surface (attested to by D_{app} and k_0 values). Additionally, values of $\Delta S^{\neq}$herein for all three electrodes decrease with increasing temperature, indicating that a certain degree of order in terms of electrostatic interactions, π-stacking, and conjugation is necessary for each deposition for electron transport. Therefore, it is plausible that intra- and inter-molecular electron hopping as opposed to a collision-dependent electron transport is the main charge transfer model. An alternative interpretation of the $\Delta S^{\neq}$variation with temperature is that the electron flux is reduced due to down-regulation of photosynthetic activity at increasing temperatures of the test window. This interpretation can be negated considering the highest current densities for the *"mixed"* and *"layered"* electrodes were recorded respectively around 42 °C and 38 °C (Fig. 5a).

$$H^{\neq} = E_a - RT \quad [6]$$

where $H^{\neq}$ is the activation enthalpy of charge transfer.

The endothermic enthalpies calculated for the charge transfer across each electrode correlate to the thermally-activated charge transfer process (Eq. 6, Table II).[56] The endothermicity increases in the order of PDHA, "*layered*," "*mixed*," indicating the higher thermodynamic energy expense (i) during photobioelectrocatalysis compared to the non-catalytic PDHA electrode, and (ii) for charge propagation across the "*mixed*" biohybrid compared to the "*layered*".[56,58]

Heterogenous rate of electron transfer (k_0) via the Laviron model.—The heterogeneous electron transfer rate constant (k_0) quantifies the rapidity of electron transfer from an electroactive species to the electrode, which is primarily a function of the distance

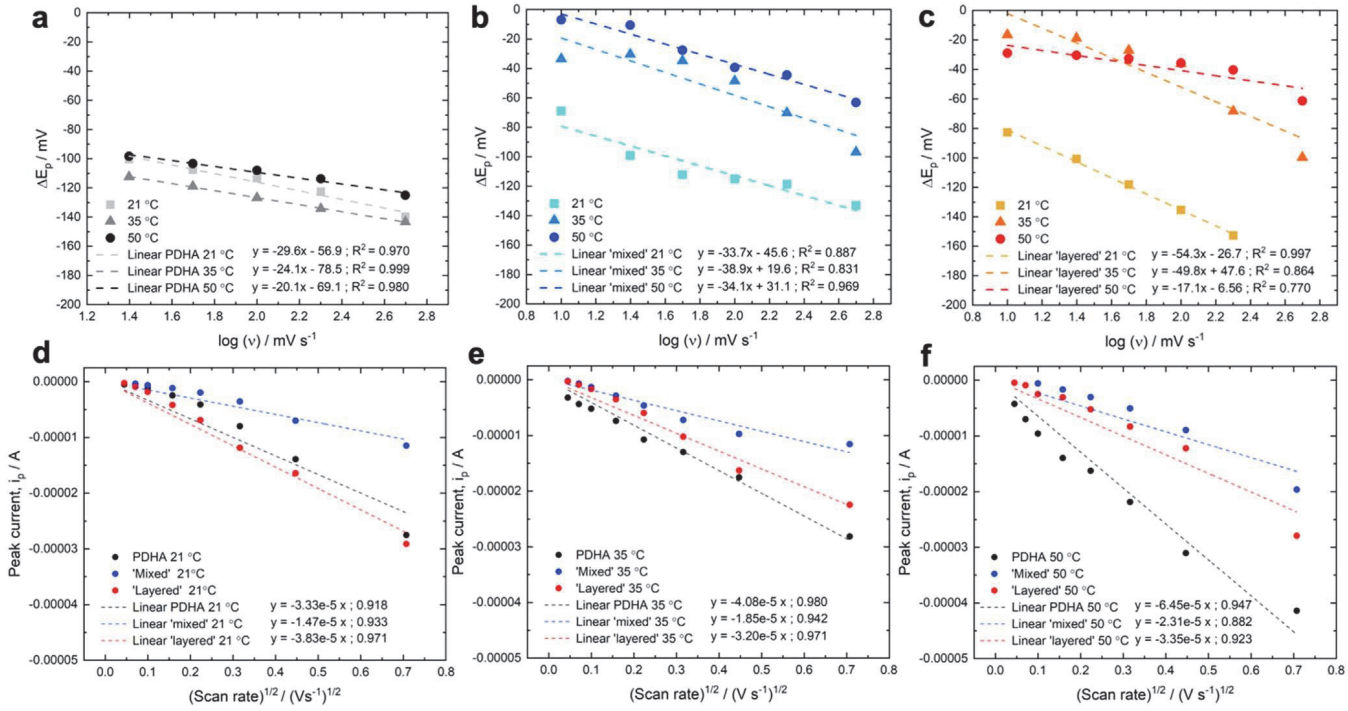

Figure 7. (a)–(c) Averaged plots of ΔE_p vs the log of scan rate for: (a) solely-PDHA electrodes, (b) "*mixed*," and (c) "*layered*" biohybrids. (d)–(f) Averaged plots of peak current vs square root of scan rate at: (d) room temperature 21 °C ± 4 °C, (e) 35 °C ± 4 °C, and (f) 50 °C ± 4 °C.

and potential difference between the two.[59] The cathodic (α_C) and anodic (α_A) charge transfer coefficients are defined as the fraction of electrostatic potential energy contributing to the cathodic and anodic reactions, respectively on each electrode.[60] The Laviron approach was used to analyze the cyclic voltammetry data to obtain α_A, α_C, (Figs. S14, Table SVI) and k_0 values (Fig. 7, Table III), based on the interim assumption that the heterogeneous electron transfer rate is not limited by the preceding step of charge transfer across the polymer.

The linearity of the graphs of the quinone peak current vs square root of scan rate for the three electrodes at 21 °C, 35 °C, and 50 °C (Fig. 7) is indicative of self-exchange-based conduction, as is typically the case with redox polymers. The quinone redox conversion of PDHA from hydroquinone to benzoquinone could potentially go through multiple semiquinone forms. Deconvoluting the exact rate-limiting step during the conversion in this scheme is difficult, due to the coupling between electron conductance and redox activity. The k_0 for "*mixed*" biohybrid reflects the inverse-trend corresponding to its R_{CT} values (Table IV). Comparatively, the k_0 for solely-PDHA and "*layered*" electrodes are not significantly affected by temperature. It was assumed that when the CRP PDHA forms a consistent conducting layer on the electrode surface, increasing the temperature to influence higher thermal motion has little effect on k_0. This assumption is based on the fact, that the higher density of percolation pathways for electron transport within compact polymer layers is a key influencing factor in heterogeneous electron transfer.[61]

Charge transfer resistance in biohybrid formulations.— Compared to direct current analysis methods, electrochemical impedance spectroscopy (EIS) is a highly informative kinetic tool to analyze complex electrochemical systems, without applying overgeneralizing assumptions. Due to the complexity of the photobioelectrocatalytic biohybrid systems, the validity of EIS data is dependent on the conditions of "*stability*," "*causality*" and "*linearity*."[62] The frequency range to acquire AC impedance data was determined considering that the: (i) timescale for photon absorption, charge separation, and fluorescence in chloroplasts are in the order of 10^{-6}–10^{-15}s,[63] (ii) timescale for electric double layer formation and electrocatalytic charge transfer are in the 10^{-6}–10^{-3}s range,[63] and (iii) mean scattering time for electron hopping within a one carbon-carbon distance in a conducting polymer approximately in the order of 2×10^{-16}s.[64] "*Stability*" is assumed by limiting the analysis to this high-frequency range, where the influence of drift is low. The graphs of open circuit potential difference vs time for biohybrids before and after impedance experiments (Fig. S15) indicate that the OCP of each system does not noticeably change with time. The small change in OCP in each system after obtaining EIS data was attributed to the passage of photobioelectrocatalytic current. Therefore, "*causality*" was indirectly assumed by the absence of auxiliary sources that influence the EIS signal. A relatively small amplitude of 0.005 V was used to ensure that no harmonics were generated during EIS ("*pseudo-linearity*").

Herein, charge transfer resistance across each electrode deposition to the electrode surface (R_{CT}) was quantified using Nyquist plots constructed from AC impedance data. Nyquist plots (Fig. S16) resolve individual charge transfer processes more easily, especially within narrow frequency ranges, compared to Bode plots. The simplest equivalent cells with the lowest error percentage for solely-chloroplast, and "*mixed*" deposition electrodes constituted the passive electrical circuit elements; double layer capacitance (C_d), charge transfer resistance (R_{CT}), constant phase element (Q), Warburg impedance (W), interfacial resistance (R_F) and interfacial capacitance (C_F) between the chloroplast/PDHA-chloroplast layer and electrode, and the uncompensated solution resistance (R_u) (Fig. 8a). Q accounts for the "imperfect" capacitor behavior of the rough, non-uniform, and geometric shape of the porous electrodes. W correlates to the general impedance for mass transfer (i.e., counter ion migration, contextually). The equivalent circuit for the "*layered*" electrode included the added elements of parallelly-connected resistance and capacitance corresponding to the additional interface introduced between the chloroplast and PDHA layers (Fig. 8b). $R_{F'}$ and $C_{F'}$ are, respectively, the resistance and capacitance at the chloroplast-PDHA interface in the "*layered*" deposition.

The R_{CT} values for the three electrodes (Table IV) consistently decreased from chloroplast electrode to "*mixed*" to "*layered*" depositions at room temperature, congruous with their photobioelectrocatalytic performance (Fig. 5). From 21 °C to 35 °C, the R_{CT} for each electrode significantly decreased, attributable to increased thermal motion. From 35 °C to 50 °C, the R_{CT} for each electrode slightly decreased, which could be attributed to deteriorating physical contact at the electrode-PDHA/chloroplast interface due to increasing thermal vibrations. The higher R_{CT} for "*mixed*" depositions compared to the chloroplast electrodes and "*layered*" depositions at 35 °C and 50 °C was possibly due to the increased electron tunneling/hopping distances. This physically significant trend of R_{CT} with varying temperatures for the biohybrid electrodes obtained via EIS is partially reflected in k_0 values obtained via the Laviron model (Table III). Additionally, the resistances estimated by EIS for charge transfer across the depositions are several orders of magnitude higher (Table SVIII) than the R_{CT} values, which indicates that measured current responses of the photobioelectrocatalytic systems are limited by the electron transfer across the depositions as opposed to heterogeneous electron transfer at the interface.

The complexity of assessing photobioelectrocatalytic electron transfer in biohybrids (i.e., "*mixed*" and "*layered*" depositions of electroactive materials) is elevated by the metabolic autonomy of chloroplasts. A few aspects of this complexity, related to chloroplasts, were not addressed in this study. For example, the lipid double layer around chloroplasts retard charge and mass transport to the photoactive redox centers.[65–67] Therefore, photoelectron transfer from chloroplasts to PDHA affects the photobioelectrocatalytic rate of the biohybrids irrespective of the deposition strategy, as also indicative by the i_K values obtained by RDE. Surface charge of chloroplast membranes increase the capacitive behavior of PDHA.[2] Consequently, increased cell time constant of each biohybrid can potentially deviate the "Cottrell conditions" assumed in the analysis of DPSCA data.[45] Photosynthetic proteins in their native environment are susceptible to participate in auxiliary biochemical processes such as; (i) chloroplast respiration, and (ii) repair mechanisms against photodamage and reactive oxygen species (ROS).[65,68] In chloroplast respiration, reduced ferredoxin in the photosynthetic electron transfer chain is intercepted by physiological acceptors in the vicinity causing side reactions.[69] While quinones are

Table III. Heterogenous electron transfer rate constant (k_0) from electroactive material deposition to electrode surface, at temperatures 21 °C ± 4 °C, 35 °C ± 4 °C, and 50 °C ± 4 °C.

Electrode	Average k_0 (s^{-1})		
	21 °C	35 °C	50 °C
PDHA electrode	0.444(±0.064)	0.436(±0.015)	0.455(±0.013)
"*Mixed*" biohybrid	0.186(±0.077)	0.353(±0.133)	0.309(±0.127)
"*Layered*" biohybrid	0.501(±0.169)	0.487(±0.115)	0.500(±0.028)

Table IV. Averaged charge transfer resistance (R_{CT}) values for the solely-chloroplast electrode, "*mixed*," and "*layered*" biohybrids, at room temperature (21 °C ± 4 °C), 35 °C ± 4 °C, and 50 °C ± 4 °C, based on equivalent circuits.

Electrode	R_{CT} (Ω cm^{-2})		
	21 °C	35 °C	50 °C
Chloroplast electrode	236 (±29)	31.1 (±3.7)	40.2 (±18.1)
"*Mixed*" biohybrid	172 (±50)	35.6 (±8.9)	53.4 (±23.0)
"*Layered*" biohybrid	37.4 (±15.9)	17.8 (±13.1)	26.5 (±15.0)

biocompatible with chloroplasts, the former can also facilitate non-specific electron extraction from vicinal redox intermediates with suitable redox potentials.[65,70] Such interferences can up- or down-regulate the photosynthetic mechanism within the biohybrids, further masking the system analysis. However, compared to quinone-based diffusible redox mediators which can interfere with other cellular electron transport processes at high concentrations, immobilized redox polymers are less invasive due to their spatial restrictions.[1] Additionally, influence of phase transition of the chloroplast lipid bilayer, conformations of chloroplast proteins, oxygen solubility, solvation of the polymer, etc. in photobioelectrocatalytic biohybrids, which are functions of temperature,[52,53] were not analyzed during the investigation of activation parameters in this study.

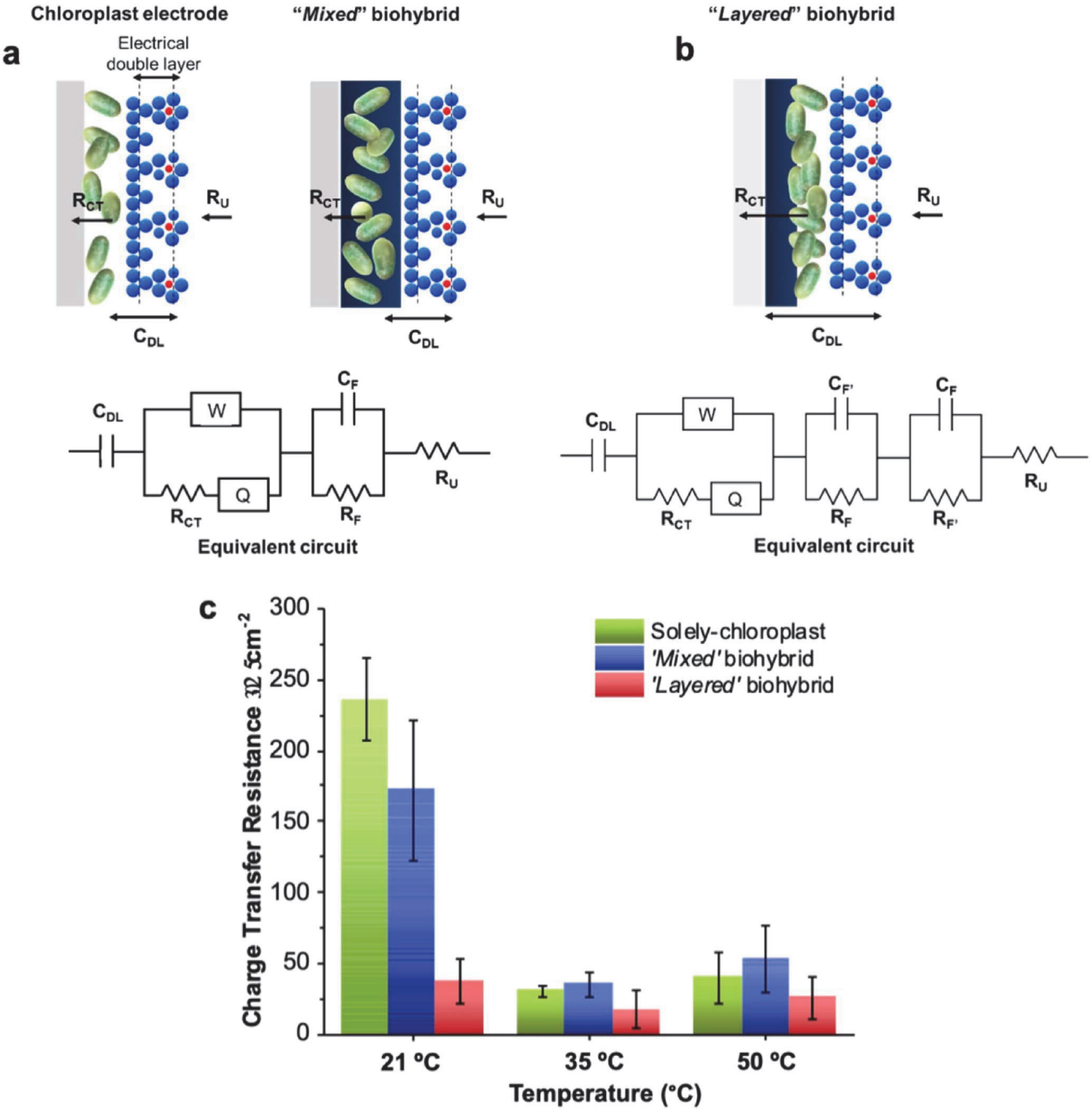

Figure 8. (a) EIS equivalent circuits for corresponding chloroplast, and "*mixed*" bioelectrode, and (b) "*layered*" bioelectrode formulations. (c) Averaged charge transfer resistance (R_{CT}) values for the solely-chloroplast electrode, "*mixed*," and "*layered*" biohybrids, at room temperature (21 °C ± 4 °C), 35 °C ± 4 °C, and 50 °C ± 4 °C, based on equivalent circuits.

Conclusions

Photobioelectrocatalytic charge transfer mechanism across biohybrid electrodes can be broadly divided into at least five interconnected steps: (i) transfer of photobiocatalytic electron flux from chloroplasts to redox mediating polymer, (ii) diffusion of the electron flux across bioelectrodes, (iii) concomitant counterion migration to maintain charge neutrality on polymer, (iv) mass transfer of reactants, and (v) heterogeneous electron transfer to the electrode.

While the presence of the CRP categorically elevates photobioelectrocatalysis achieved by intact chloroplasts, the "*layered*" deposition strategy of the CRP and biocatalyst creates the optimal architecture of electron-source, -bridge, and -sink. The superior photobioelectrocatalytic performance at the biotic-abiotic interface in the "*layered*" biohybrid was quantified in terms of rate (D_{app}), thermodynamic and kinetic barriers ($H^{\neq}$, E_a), frequency of molecular collisions (D_0) during electron transport across depositions, and rate and resistance to heterogeneous electron transfer (k_0, R_{CT}). Both steady-state and transient diffusion measurements were synchronously utilized to quantify D_{app} to: (i) account for both electron and ion transport, and (ii) discern the effective concentration of PDHA in electrical communication, in each electrode. The higher D_{app} in the "*layered*" biohybrid is a manifestation of: (i) faster charge mobility across the CRP bridge, (ii) steep photoelectron gradient generated by the localization of chloroplasts as a surface layer to absorb light, unimpeded by the black PDHA, (iii) superior surface adhesion of electroactive material, and (iv) efficient heterogeneous electron transfer due to a higher density of percolation pathways in the absence of interspersed insulating chloroplasts. Values of D_{app} were calculated assuming that of the listed five major steps of charge transfer, electron transport across the electroactive material is the kinetically slow rate-limiting step. This assumption was experimentally justified by the: (i) R_F values obtained via EIS being several orders of magnitude higher than R_{CT} values, (ii) positive values of $\Delta S^{\neq}$, and (iii) i_K values obtained via the Koutecky-Levich model. Comparatively, mass transfer where water is the oxidized substrate, and counterion migration wherein the major counterion is highly mobile protons, are auxiliary steps in terms of the rate of the overall mechanism. Further experimentation is required to deconvolute the contribution by photoelectron transfer from chloroplasts to polymer in "*mixed*" and "*layered*" biohybrids, during this rate-limiting step across the electroactive material. Effective concentration of PDHA in electrical communication determined by diffusion measurements is higher than the polaron concentration for PDHA determined by EPR. Therefore, the major charge carrier in the CRP systems are electrons as opposed to polarons in CPs and branched CRPs (i.e., unbranched CRPs function more as RPs than CPs). Values of $\Delta S^{\neq}$ indicate that a certain degree of structural organization is required for the thermally activated charge transfer process. Therefore, electron transport across the biohybrids favor intra- and intermolecular electron hopping as opposed to collision-based transport through PDHA.

Further studies on the (i) transfer of catalytic photoelectron flux from chloroplasts to CRPs and (ii) purported superior light absorption by the "*layered*" biohybrid than the "*mixed*" counterpart can be conducted via photo-action spectra. Understanding the double layer formation and potential distribution at the CRP-photobiocatalyst interface via methods such as in situ vibrational Stark spectroscopy would also be instrumental in this regard. Supplementary techniques such as chronoabsorptiometry,[15] transient absorption spectroscopy[71] and indirect laser-induced temperature jump measurements[72] can be used to probe more in-depth charge transfer dynamics between the photobiocatalyst and polymer by obtaining lifetime measurements of photoelectrons and corresponding rate constants. Investigating the effect of applied electric field on the redox conductivity in CRPs and across the biohybrids remains to be investigated (e.g., using Tafel plots, EIS). Ultramicroelectrodes such as interdigitated array electrodes, which generate relatively high Faradaic current density against the charging current density, can be used to reduce the high signal-to-noise ratios obtained in steady state conditions via RDE.[46] Thickness optimization of the PDHA layer is crucial considering that electron hopping is the major electron transport mechanism in the "*layered*" deposition, and the electron hopping rate exponentially decays with distance (β).[71] Quantifying the differential tortuosity of the "*layered*" and "*mixed*" biohybrids using isotherms or X-ray tomographic microscopy in conjunction with numerical diffusion simulations,[73] can provide a more realistic mechanistic image of the heterogenous microporous electrode surface with varying the electroactive area. Effect of decimal-level changes in neutral pH of the electrolyte to the mobility of polymer redox centers, H^+ availability, film expansion by electrostatic repulsion, doping of redox polymer would also be insightful.

Effective CRP-photobiocatalyst biohybrid designs require a holistic approach that transcends the chemical structure of CRP and thermodynamics of electron transfer. "Electrochemically-*wiring*" electrodes and photobiocatalysts entail tailoring the abiotic-biotic interface during photocurrent generation. Photobioelectrocatalysis at this interface is influenced by a summation of factors including, but not limited to: (i) chemical and electronic structure of the polymer, (ii) deposition strategy (e.g., structure, morphology, thickness) to better emulate the mean redox polymeric properties of unbranched CRP, (iii) exposure to physiologically significant elements (e.g., light, temperature), (iv) ionic, electronic and substrate composition in the electrolyte that imbibes the interface, and (v) applied electrochemical potential. Incisive design and formulation of these biohybrids for optimal photobioelectrocatalysis requires further studies that dissect biotic-abiotic interfaces and monitor the synchronous effect of modulating a single parameter on multiple levels of inherently and increasingly complex biohybrids, based on rational assumptions.

Acknowledgments

This work made use of the University of Utah USTAR shared facilities supported, in part, by the MRSEC program of NSF under Award No. DMR-1121252. The authors gratefully acknowledge funding from the Office of Naval Research (Grant #N00014-21-1-4008) and National Science Foundation (Grant #1921075 and #1922956). O.S. acknowledges support from the Irving S. Sigal Postdoctoral Fellowship by the American Chemical Society. The authors gratefully acknowledge Prof. Joel Harris from the Department of Chemistry, University of Utah for his contribution in analyzing the confocal Raman microscopy data for this study.

ORCID

N. Samali Weliwatte https://orcid.org/0000-0002-2989-8884
Olja Simoska https://orcid.org/0000-0001-5356-721X
Daniel Powell https://orcid.org/0000-0002-5893-0695
Miharu Koh https://orcid.org/0000-0001-9677-2504
Matteo Grattieri https://orcid.org/0000-0002-1795-3655
Luisa Whittaker-Brooks https://orcid.org/0000-0002-1130-1306
Carol Korzeniewski https://orcid.org/0000-0003-3672-0731
Shelley D. Minteer https://orcid.org/0000-0002-5788-2249

References

1. N. S. Weliwatte, M. Grattieri, and S. D. Minteer, "Rational design of artificial redox-mediating systems toward upgrading photobioelectrocatalysis." *Photochemical & Photobiological Sciences*, **20**, 1333 (2021).
2. N. S. Weliwatte, M. Grattieri, O. Simoska, Z. Rhodes, and S. D. Minteer, "Unbranched hybrid conducting redox polymers for intact chloroplast-based photobioelectrocatalysis." *Langmuir*, **37**, 7821 (2021).
3. M. Grattieri, Z. Rhodes, D. P. Hickey, K. Beaver, and S. D. Minteer, "Understanding biophotocurrent generation in photosynthetic purple bacteria." *ACS Catal.*, **9**, 867 (2019).
4. F. Giroud, R. D. Milton, B.-X. Tan, and S. D. Minteer, "Simplifying enzymatic biofuel cells: immobilized naphthoquinone as a biocathodic orientational moiety and bioanodic electron mediator." *ACS Catal.*, **5**, 1240 (2015).

5. I. Mazurenko, V. P. Hitaishi, and E. Lojou, "Recent advances in surface chemistry of electrodes to promote direct enzymatic bioelectrocatalysis." *Current Opinion in Electrochemistry*, **19**, 113 (2020).
6. G. Pankratova and L. Gorton, "Electrochemical communication between living cells and conductive surfaces." *Current Opinion in Electrochemistry*, **5**, 193 (2017).
7. D. Voiry, H. S. Shin, K. P. Loh, and M. Chhowalla, "Low-dimensional catalysts for hydrogen evolution and CO_2 reduction." *Nature Reviews Chemistry*, **2**, 0105 (2018).
8. R. D. Milton, D. P. Hickey, S. Abdellaoui, K. Lim, F. Wu, B. Tan, and S. D. Minteer, "Rational design of quinones for high power density biofuel cells." *Chem. Sci.*, **6**, 4867 (2015).
9. H. Chen et al., "Fundamentals, applications, and future directions of bioelectrocatalysis." *Chem. Rev.*, **120**, 12903 (2020).
10. R. D. Milton, T. Wang, K. L. Knoche, and S. D. Minteer, "Tailoring biointerfaces for electrocatalysis." *Langmuir*, **32**, 2291 (2016).
11. Y. Hu and C. M. Niemeyer, "From DNA nanotechnology to material systems engineering." *Adv. Mater.*, **31**, 1806294 (2019).
12. A. Heller, "Electron-conducting redox hydrogels: design, characteristics and synthesis." *Curr. Opin. Chem. Biol.*, **10**, 664 (2006).
13. A. Aoki and A. Heller, "Electron diffusion coefficients in hydrogels formed of cross-linked redox polymers." *J. Phys. Chem.*, **97**, 11014 (1993).
14. E. F. Dalton, N. A. Surridge, J. C. Jernigan, K. O. Wilbourn, J. S. Facci, and R. W. Murray, "Charge transport in electroactive polymers consisting of fixed molecular redox sites." *Chem. Phys.*, **141**, 143 (1990).
15. J. M. Cardon, G. Krueper, R. Kautz, D. M. Fabian, J. Angsono, H.-Y. Chen, and S. Ardo, "Reconciliation of differences in apparent diffusion coefficients measured for self-exchange electron transfer between molecules anchored to mesoporous titanium dioxide thin films." *ACS Appl. Mater. Interfaces*, **13**, 41396 (2021).
16. K. Asadi, A. J. Kronemeijer, T. Cramer, L. Jan Anton Koster, P. W. M. Blom, and D. M. de Leeuw, "Polaron hopping mediated by nuclear tunnelling in semiconducting polymers at high carrier density." *Nat. Commun.*, **4**, 1710 (2013).
17. C. Cobet, J. Gasiorowski, D. Farka, and P. Stadler, "Polarons in conjugated polymers." *In Ellipsometry of Functional Organic Surfaces and Films* (Springer, Berlin) pp 355 (2018).
18. S. D. Kang and G. J. Snyder, "Charge-transport model for conducting polymers." *Nat. Mater.*, **16**, 252 (2017).
19. K. Sato, R. Ichinoi, R. Mizukami, T. Serikawa, Y. Sasaki, J. Lutkenhaus, H. Nishide, and K. Oyaizu, "Diffusion-cooperative model for charge transport by redox-active nonconjugated polymers." *JACS*, **140**, 1049 (2018).
20. H. Huang, C. Karlsson, F. Mamedov, M. Strømme, A. Gogoll, and M. Sjödin, "Polaron disproportionation charge transport in a conducting redox polymer." *The Journal of Physical Chemistry C*, **121**, 13078 (2017).
21. M. Sterby, R. Emanuelsson, F. Mamedov, M. Strømme, and M. Sjödin, "Investigating electron transport in a PEDOT/Quinone conducting redox polymer with in situ methods." *Electrochim. Acta*, **308**, 277 (2019).
22. R. Zahn, G. Coullerez, J. Vörös, and T. Zambelli, "Effect of polyelectrolyte interdiffusion on electron transport in redox-active polyelectrolyte multilayers." *J. Mater. Chem.*, **22**, 11073 (2012).
23. M. Grattieri, S. Patterson, J. Copeland, K. Klunder, and S. D. Minteer, "Purple bacteria and 3D redox hydrogels for bioinspired photo-bioelectrocatalysis." *ChemSusChem*, **13**, 230 (2020).
24. A. Vlad, K. Arnould, B. Ernould, L. Sieuw, J. Rolland, and J.-F. Gohy, "Exploring the potential of polymer battery cathodes with electrically conductive molecular backbone." *J. Mater. Chem. A*, **3**, 11189 (2015).
25. L. Sieuw, B. Ernould, J.-F. Gohy, and A. Vlad, "On the improved electrochemistry of hybrid conducting-redox polymer electrodes." *Sci. Rep.*, **7**, 4847 (2017).
26. S. R. Kargirwar and S. Kondawar, "Fluorescence study of polyaniline doped with organic acids." *Asian Journal of Research in Chemistry*, **8**, 36 (2015).
27. P. A. Webb, "Volume and density determinations for particle technologists." *Micromeritics Instrument Corp*, **2**, 01 (2001).
28. B. Yurash et al., "Towards Understanding the doping mechanism of organic semiconductors by lewis acids." *Nat. Mater.*, **18**, 1327 (2019).
29. E. S. Matveeva, "Could the acid doping of polyaniline represent the charge transfer interaction ? " *Synth. Met.*, **83**, 89 (1996).
30. C. P. Andrieux and J. Saveant, "Electroneutrality coupling of electron hopping between localized sites with electroinactive counterion displacement. 1. potential-step plateau currents." *J. Phys. Chem.*, **92**, 6761 (1988).
31. E. Laviron, "General expression of the linear potential sweep voltammogram in the case of diffusionless electrochemical systems." *J. Electroanal. Chem. Interfacial Electrochem.*, **101**, 19 (1979).
32. W. S. Chow, "Photosynthesis: from natural towards artificial." *J. Biol. Phys.*, **29**, 447 (2003).
33. E. Nagy, "2 - Molecular diffusion." *Basic Equations of the Mass Transport through a Membrane Layer*, ed. E. Nagy (Elsevier, Oxford, Amsterdam) pp 35 (2012).
34. K. Krikstopaitis and J. Kulys, "Electrochemical properties of violuric acid and oxidase biosensor preparation." *Electrochem. Commun.*, **2**, 119 (2000).
35. G. Karim-Nezhad, M. Hasanzadeh, L. Saghatforoush, N. Shadjou, S. Earshad, and B. Khalilzadeh, "Kinetic study of electrocatalytic oxidation of carbohydrates on cobalt hydroxide modified glassy carbon electrode." *J. Braz. Chem. Soc.*, **20**, 141 (2009).
36. D. Thomas, Z. Rasheed, J. S. Jagan, and K. G. Kumar, "Study of kinetic parameters and development of a voltammetric sensor for the determination of butylated hydroxyanisole (BHA) in oil samples." *J. Food Sci. Technol.*, **52**, 6719 (2015).
37. K. Sjoholm, M. Cooney, and S. Minteer, "Biocompatible micellar environment for enzyme encapsulation for bioelectrocatalysis applications." *ECS Trans.*, **19**, 1 (2019).
38. B. A. Gregg and A. Heller, "Redox polymer films containing enzymes. 1. A redox-conducting epoxy cement: synthesis, characterization, and electrocatalytic oxidation of hydroquinone." *J. Phys. Chem.*, **95**, 5970 (1991).
39. P. Pickup and R. W. Murray, "Redox conduction in mixed-valent polymers." *JACS*, **105**, 4510 (1983).
40. G. L. Turdean, I. C. Popescu, L. Oniciu, and D. R. Thevenot, "Sensitive detection of organophosphorus pesticides using a needle type amperometric acetylcholinesterase-based bioelectrode. thiocholine electrochemistry and immobilised enzyme inhibition." *J. Enzyme Inhib. Med. Chem.*, **17**, 107 (2002).
41. M. H. A. Zavar, S. Heydari, and G. H. Rounaghi, "Electrochemical determination of salicylic acid at a new biosensor based on polypyrrole-banana tissue composite." *Arab. J. Sci. Eng.*, **38**, 29 (2013).
42. M. R. Majidi, K. Asadpour-Zeynali, and S. Gholizadeh, "Amperometric biosensor for dopamine determination based on over-oxidized polypyrrole-plant tissue composite." *Int. J. Polym. Anal. Charact.*, **14**, 89 (2009).
43. C. Tortolini, S. Rea, E. Carota, S. Cannistraro, and F. Mazzei, "Influence of the immobilization procedures on the electroanalytical performances of trametes versicolor laccase based bioelectrode." *Microchem. J.*, **100**, 8 (2012).
44. R. J. Forster, A. J. Kelly, J. G. Vos, and M. E. G. Lyons, "The effect of supporting electrolyte and temperature on the rate of charge propagation through thin films of [Os(bipy)2PVP10Cl]Cl coated on stationary electrodes." *J. Electroanal. Chem. Interfacial Electrochem.*, **270**, 365 (1989).
45. A. J. Bard and L. R. Faulkner, "Fundamentals and applications." *Electrochemical Methods*, **2**, 580 (2001).
46. T. Kothe, S. Pöller, F. Zhao, P. Fortgang, M. Rögner, W. Schuhmann, and N. Plumeré, "Engineered electron-transfer chain in photosystem 1 based photocathodes outperforms electron-transfer rates in natural photosynthesis." *Chemistry —A European Journal*, **20**, 11029 (2014).
47. Y. Suzuki, K. Kano, O. Shirai, and Y. Kitazumi, "Diffusion-limited electrochemical D-fructose sensor based on direct electron transfer-type bioelectrocatalysis by a variant of D-fructose dehydrogenase at a porous gold microelectrode." *J. Electroanal. Chem.*, **877**, 114651 (2020).
48. M. E. G. Lyons, H. G. Fay, J. G. Vos, and A. J. Kelly, "Temperature dependence of charge transport processes in surface deposited redox polymer layers." *J. Electroanal. Chem. Interfacial Electrochem.*, **250**, 207 (1988).
49. C. Canali, C. Jacoboni, F. Nava, G. Ottaviani, and A. Alberigi-Quaranta, "Electron drift velocity in silicon." *Physical Review B*, **12**, 2265 (1975).
50. V. Krinichnyi, H.-K. Roth, G. Hinrichsen, F. Lux, and K. Lüders, "EPR and charge transfer in H2SO4-doped polyaniline." *Physical Review B*, **65**, 155205 (2002).
51. D. T. Wilkinson and H. R. Crane, "Precision measurement of the g factor of the free electron." *Phys. Rev.*, **130**, 852 (1963).
52. S. Dutta, S. Mohanty, and B. C. Tripathy, "Role of temperature stress on chloroplast biogenesis and protein import in pea." *Plant Physiol.*, **150**, 1050 (2009).
53. W. G. Nolan and R. M. Smillie, "Multi-temperature effects on hill reaction activity of barley chloroplasts." *Biochimica et Biophysica Acta (BBA) - Bioenergetics*, **440**, 461 (1976).
54. Q. Zhang, Y. Sun, W. Xu, and D. Zhu, "Thermoelectric materials: organic thermoelectric materials: emerging green energy materials converting heat to electricity directly and efficiently (Adv. Mater. 40/2014)." *Adv. Mater.*, **26**, 6828 (2014).
55. P. Daum, J. Lenhard, D. Rolison, and R. W. Murray, "Diffusional charge transport through ultrathin films of radiofrequency plasma polymerized vinylferrocene at low temperature." *JACS*, **102**, 4649 (1980).
56. L. Sun, K. Jiao, and S. G. Weber, "Charge transport through osmium-containing redox polymers in nitrophenyl-based solvents: effect of solvent size." *J. Phys. Chem. B*, **102**, 1945 (1998).
57. C. Alemán, C. A. Ferreira, J. Torras, A. Meneguzzi, M. Canales, M. A. S. Rodrigues, and J. Casanovas, "On the molecular properties of polyaniline: a comprehensive theoretical study." *Polymer*, **49**, 5169 (2008).
58. R. J. Forster, J. G. Vos, and M. E. G. Lyons, "Controlling processes in the rate of charge transport through [Os(bipy)2(PVP)Cl]Cl redox polymer-modified electrodes." *J. Chem. Soc., Faraday Trans.*, **87**, 3761 (1991).
59. A. A. S. Gietter, R. C. Pupillo, G. P. A. Yap, T. P. Beebe, J. Rosenthal, and D. A. Watson, "On-surface cross-coupling methods for the construction of modified electrode assemblies with tailored morphologies." *Chem. Sci.*, **4**, 437 (2013).
60. Jean-Michel Savéant and Didier Tessier, "Variation of the electrochemical transfer coefficient with potential." *Faraday Discussions of the Chemical Society*, **74**, 57 (1982).
61. K. Wijeratne, U. Ail, R. Brooke, M. Vagin, X. Liu, M. Fahlman, and X. Crispin, "Bulk electronic transport impacts on electron transfer at conducting polymer electrode–electrolyte interfaces." *Proc. Natl Acad. Sci.*, **115**, 11899 (2018).
62. Gamry Instruments, (2007), Complex impedance in CorrosionBasics of electrochemical impedance spectroscopy https://www.gamry.com/application-notes/EIS/basics-of-electrochemical-impedance-spectroscopy/.
63. N. Wagner, *Introduction to Electrochemical Impedance Spectroscopy (EIS).* (2014).
64. A. J. Heeger, "Charge transfer in conducting polymers. striving toward intrinsic properties." *Faraday Discuss. Chem. Soc.*, **88**, 203 (1989).
65. M. Grattieri, K. Beaver, E. M. Gaffney, F. Dong, and S. D. Minteer, "Advancing the fundamental understanding and practical applications of photo-bioelectrocatalysis." *Chem. Commun.*, **56**, 8553 (2020).
66. L. Beauzamy, J. Delacotte, B. Bailleul, K. Tanaka, S. Nakanishi, F.-A. Wollman, and F. Lemaître, "Mediator-microorganism interaction in microbial solar cell: a fluo-electrochemical insight." *Anal. Chem.*, **92**, 7532 (2020).
67. O. Aleksejeva, N. Nilsson, V. Genevskiy, K. Thulin, and S. Shleev, "Photobioanodes based on nanoimprinted electrodes and immobilized chloroplasts." *ChemElectroChem*, **9**, e202101219 (2022).

68. M. Edelman and A. K. Mattoo, "D1-protein dynamics in photosystem II: the lingering enigma." *Photosynth. Res.*, **98**, 609 (2008).
69. Y. W. Kow, D. L. Erbes, and M. Gibbs, "Chloroplast respiration 1: a means of supplying oxidized pyridine nucleotide for dark chloroplastic metabolism." *Plant Physiol.*, **69**, 442 (1982).
70. N. Schuergers, C. Werlang, C. M. Ajo-Franklin, and A. A. Boghossian, "A synthetic biology approach to engineering living photovoltaics." *Energy Environ. Sci.*, **10**, 1102 (2017).
71. E. M. Conwell and S. V. Rakhmanova, "Polarons in DNA." *Proc. Natl Acad. Sci.*, **97**, 4556 (2000).
72. H. D. Sikes, J. F. Smalley, S. P. Dudek, A. R. Cook, M. D. Newton, C. E. D. Chidsey, and S. W. Feldberg, "Rapid electron tunneling through oligophenylenevinylene bridges." *Science*, **291**, 1519 (2001).
73. B. Suthar, J. Landesfeind, A. Eldiven, and H. A. Gasteiger, "Method to determine the in-plane tortuosity of porous electrodes." *J. Electrochem. Soc.*, **165**, A2008 (2018).